

## Using simultaneous PET/MRI to compare the accuracy of diagnosing frontotemporal dementia by arterial spin labelling MRI and FDG-PET

Udunna C. Anazodo<sup>a,b,\*</sup>, Elizabeth Finger<sup>c</sup>, Benjamin Yin Ming Kwan<sup>d</sup>, William Pavlosky<sup>a,d</sup>, James Claude Warrington<sup>d</sup>, Matthias Günther<sup>e,f</sup>, Frank S. Prato<sup>a,b</sup>, Jonathan D. Thiessen<sup>a,b</sup>, Keith S. St. Lawrence<sup>a,b</sup>

<sup>a</sup> Lawson Health Research Institute, St Joseph's Health Care, 268 Grosvenor St., London, Ontario N6A 4V2, Canada

<sup>b</sup> Department of Medical Biophysics, Schulich School of Medicine and Dentistry, Western University, Medical Sciences Building, Rm M407, London, Ontario N6A 5C1, Canada

<sup>c</sup> Department of Clinical Neurological Sciences, Western University, 339 Windermere Road, London, Ontario N6A 5A5, Canada

<sup>d</sup> Department of Medical Imaging, Schulich School of Medicine and Dentistry, Western University, London, Ontario N6A 5W9, Canada

<sup>e</sup> Fraunhofer Institute for Medical Image Computing MEVIS, Am Fallturm 1, 28359 Bremen, Germany.

<sup>f</sup> University Bremen, Faculty 1, Otto-Hahn-Allee 1, 28359 Bremen, Germany

### ARTICLE INFO

#### Keywords:

Arterial spin labelling MRI  
FDG-PET  
Frontotemporal dementia  
Hybrid PET/MRI

### ABSTRACT

**Purpose:** The clinical utility of FDG-PET in diagnosing frontotemporal dementia (FTD) has been well demonstrated over the past decades. On the contrary, the diagnostic value of arterial spin labelling (ASL) MRI – a relatively new technique – in clinical diagnosis of FTD has yet to be confirmed. Using simultaneous PET/MRI, we evaluated the diagnostic performance of ASL in identifying pathological abnormalities in FTD (FTD) to determine whether ASL can provide similar diagnostic value as FDG-PET.

**Methods:** ASL and FDG-PET images were compared in 10 patients with FTD and 10 healthy older adults. Qualitative and quantitative measures of diagnostic equivalency were used to determine the diagnostic utility of ASL compared to FDG-PET. Sensitivity, specificity, and inter-rater reliability were calculated for each modality from scores of subjective visual ratings and from analysis of regional mean values in thirteen a priori regions of interest (ROI). To determine the extent of concordance between modalities in each patient, individual statistical maps generated from comparison of each patient to controls were compared between modalities using the Jaccard similarity index (JI).

**Results:** Visual assessments revealed lower sensitivity, specificity and inter-rater reliability for ASL (66.67%/62.12%/0.2) compared to FDG-PET (88.43%/90.91%/0.61). Across all regions, ASL performed lower than FDG-PET in discriminating patients from controls (areas under the receiver operating curve: ASL = 0.75 and FDG-PET = 0.87). In all patients, ASL identified patterns of reduced perfusion consistent with FTD, but areas of hypometabolism exceeded hypoperfused areas (group-mean JI = 0.30 ± 0.22).

**Conclusion:** This pilot study demonstrated that ASL can detect similar spatial patterns of abnormalities in individual FTD patients compared to FDG-PET, but its sensitivity and specificity for discriminant diagnosis of a patient from healthy individuals remained unmatched to FDG-PET. Further studies at the individual level are required to confirm the clinical role of ASL in FTD management.

### 1. Introduction

Frontotemporal dementia (FTD) is a progressive neurodegenerative disorder associated with atrophy of the frontal and temporal lobes and is characterized by impairments in behaviour and language (Weder et al., 2007). In adults 65 years or younger, FTD is the second most

common form of early-onset neurodegenerative dementia (Onyike and Diehl-Schmid, 2013). Diagnosis of FTD is often challenging, as symptoms and features can overlap with those of Alzheimer's disease (AD) and psychiatric conditions such as late-onset schizophrenia and bipolar disorders (Weder et al., 2007). This diagnostic challenge, coupled with rapid functional decline and relatively short survival rate (3–14 years

\* Corresponding author at: Lawson Health Research Institute, St Joseph's Health Care, 268 Grosvenor St., London, Ontario N6A 4V2, Canada.

E-mail addresses: [uanazodo@lawsonimaging.ca](mailto:uanazodo@lawsonimaging.ca) (U.C. Anazodo), [Elizabeth.Finger@lhsc.on.ca](mailto:Elizabeth.Finger@lhsc.on.ca) (E. Finger), [William.Pavlosky@lawsonimaging.ca](mailto:William.Pavlosky@lawsonimaging.ca) (W. Pavlosky), [bkwan3@uwo.ca](mailto:bkwan3@uwo.ca) (J.C. Warrington), [Matthias.guenther@mevis.fraunhofer.de](mailto:Matthias.guenther@mevis.fraunhofer.de) (M. Günther), [prato@lawsonimaging.ca](mailto:prato@lawsonimaging.ca) (F.S. Prato), [jthiessen@lawsonimaging.ca](mailto:jthiessen@lawsonimaging.ca) (J.D. Thiessen), [kstlaw@lawsonimaging.ca](mailto:kstlaw@lawsonimaging.ca) (K.S. St. Lawrence).

<https://doi.org/10.1016/j.nicl.2017.10.033>

Received 20 July 2017; Received in revised form 24 October 2017; Accepted 28 October 2017

Available online 31 October 2017

2213-1582/ © 2017 The Author(s). Published by Elsevier Inc. This is an open access article under the CC BY-NC-ND license (<http://creativecommons.org/licenses/by-nc-nd/4.0/>).

from symptom onset (Onyike and Diehl-Schmid, 2013)), highlights the need for identification of sensitive biomarkers to improve early diagnosis of FTD, which can also be used for monitoring disease progression and treatment outcomes.

Cerebral glucose metabolism (CMRglc) measured using  $^{18}\text{F}$ -fluorodeoxyglucose (FDG) and positron emission tomography (PET) is an established biomarker for accurate ante-mortem diagnosis of FTD (Diehl-Schmid et al., 2007; Dukart et al., 2011; Foster et al., 2007; Ishii et al., 1998; Tosun et al., 2016) and for distinguishing FTD from other dementias (Foster et al., 2007; Tosun et al., 2016). A 2005 consensus report prepared by the Neuroimaging Work Group of the Alzheimer's Association concluded that FDG-PET is helpful for differentiating FTD from AD (Albert et al., 2005). In the US, costs for FDG-PET scans for differential diagnosis of FTD have been covered nationwide via Medicare benefits for the past 7 years (Centers for Medicare & Medicaid Services, 2009). Recently, a number of studies have shown that the MRI-based perfusion technique arterial spin labelling (ASL) can potentially provide comparable diagnostic information to FDG-PET in both FTD (Fällmar et al., 2017; Moodley et al., 2015; Tosun et al., 2016; Verfaillie et al., 2015) and AD (Musiek et al., 2012; Vercllytte et al., 2015) patients due to the coupling of perfusion to glucose metabolism (Anazodo et al., 2015; Cha et al., 2013). Since ASL is completely non-invasive – using endogenous blood-water as a flow contrast – it offers an appealing opportunity for cost-effective monitoring of FTD progression and treatment outcomes, free from the radiation burden of PET. Additionally, it frees PET for use in studies involving targeted tracers of pathophysiology, such as tau protein or neuroinflammation markers.

However, the reported sensitivity and specificity of ASL-CBF compared to FDG-PET in FTD studies vary widely, with some studies showing agreement with FDG-PET (Tosun et al., 2016; Verfaillie et al., 2015), better specificity than FDG-PET (Fällmar et al., 2017), and no added benefit of ASL (Binnewijzend et al., 2013; Bron et al., 2014). These conflicting findings are possibly due to heterogeneity of relatively small sample populations, variations in ASL techniques, and inherent limitations with sequential PET and MRI acquisitions. Errors in spatial registration and differences in brain states between separate PET and MRI scans are minimized by simultaneous imaging leading to stronger association between ASL-CBF and FDG-PET (Anazodo et al., 2015). Given the nature of FTD disease progression, accurate sequential evaluation of perfusion to glucose metabolism in FTD patients using ASL and FDG-PET can be limited if PET and MRI data are acquired a few months apart (Teipel et al., 2015). To circumvent this issue, this study utilized simultaneous PET/MR imaging to evaluate regional coupling of ASL-CBF to FDG-PET in patients with FTD. This analysis was conducted at group and single-subject level to determine if ASL-CBF performed equally well to FDG-PET for clinical diagnosis of FTD. Because FDG-PET is now clinically used to evaluate FTD on a single-subject basis, emphasis was placed on comparing diagnostic performance of ASL-CBF and FDG-PET at the individual level. Specificity and sensitivity of ASL-CBF were compared to FDG-PET using receiver operating characteristic (ROC) curve analysis, visual rating reports from trained readers, and statistical *t*-score maps.

## 2. Materials and methods

### 2.1. Participants

This study was approved by the Western University Health Sciences Research Ethics Board and conducted in accordance with the Declaration of Helsinki ethical standards. All participants provided written informed consent. The study cohort included 10 neurologically healthy controls and 11 patients with FTD recruited from the Cognitive Neurology and Aging Brain clinics at Parkwood Hospital (London, ON) between January 2014 and October 2014. Of the 11 patients, 7 were diagnosed with bvFTD (including 2 with right temporal variant bvFTD), 1 patient met criteria for bvFTD and non-fluent primary progressive

**Table 1**  
Summary of participant demographics (mean  $\pm$  standard deviation).

	bvFTD	Controls
Demographics		
Age (years)	66.3 $\pm$ 6.62	67 $\pm$ 6.62
Gender (males)	5	4
Years of illness	5.30 $\pm$ 2.50	–
Education (years)	13.10 $\pm$ 2.56	12.60 $\pm$ 2.50
Cognitive testing		
MOCA	17.57 $\pm$ 7.52	28.20 $\pm$ 1.75 <sup>§</sup>
MMSE	21.25 $\pm$ 8.35	29.40 $\pm$ 0.97 <sup>§</sup>
Prose delay	5.22 $\pm$ 3.95	8.89 $\pm$ 2.61 <sup>§</sup>
Prose immediate	4.13 $\pm$ 2.33	9.40 $\pm$ 2.94 <sup>§</sup>
Trail Making Test A	7.60 $\pm$ 4.40	8.88 $\pm$ 2.75 <sup>§</sup>
Trail Making Test B	8.20 $\pm$ 4.56	7.25 $\pm$ 0.35
Naming aphasia	5.50 $\pm$ 3.90	9.25 $\pm$ 2.54
Semantic fluency	5.83 $\pm$ 3.88	9.57 $\pm$ 2.56 <sup>§</sup>
Phonemic fluency	6.40 $\pm$ 4.07	9.25 $\pm$ 2.64 <sup>§</sup>
Clock command	7.15 $\pm$ 4.55	8.50 $\pm$ 2.12 <sup>§</sup>
Clock copy	7.50 $\pm$ 4.37	8.88 $\pm$ 2.25
Neuroimaging		
Global GM-CBF (ml/100 g/min)	31.21 $\pm$ 8.50	42.30 $\pm$ 15.65
Global GM-FDG (SUV)	0.43 $\pm$ 0.11	0.40 $\pm$ 0.08

<sup>§</sup> Statistical significance set at  $p < 0.05$ .

aphasia (nvPPA), 1 patient was diagnosed with semantic variant PPA (svPPA) with behavioural features and significant left and right temporal atrophy), and 2 patients were diagnosed with possible bvFTD (based on presence of clinical symptoms and cognitive testing profile but normal structural MRI imaging). All participants were free from confounding neurological diseases or psychiatric disorders (i.e. stroke, multiple sclerosis, brain tumor, bipolar disorder, schizophrenia, current major depression). All patients met the International consensus criteria for bvFTD or semantic variant PPA (Gorno-Tempini et al., 2011; Rascovsky et al., 2011) based on their clinical evaluation, neurocognitive testing performance (Table 1), clinical MRI brain imaging and genetic testing. Participants completed standard clinical neuropsychological assessments including Mini-Mental State Examination (MMSE) (Folstein et al., 1975), Montreal Cognitive Assessment (MoCA) (Nasreddine et al., 2005), tests for memory (prose recall), language/verbal fluency (semantic and phonemic, and naming from the Western Aphasia Battery), visuospatial skills (clock drawing tests), and attention (Trail Making Tests A and B), as outlined in an earlier study (Coleman et al., 2017). The clinical MRI scans, neurology history examination and neurocognitive testing used in diagnosis of FTD were completed within 2–4 weeks of PET/MRI scanning. Since, PET/MRI is not approved clinically in Canada for diagnosis of dementias, no FDG-PET scans were available at the time of clinical diagnosis.

### 2.2. PET/MRI acquisition

Serial MRI sequences were acquired during 60 min of dynamic PET acquisition on an integrated PET/(3 T) MRI scanner (Biograph mMR, Siemens Healthineers, Erlangen, Germany) using a 12-channel PET-compatible head coil. To minimize head motion, an immobilizing foam head mold was used (Smithers Medical Products, Alpha Cradle). List-mode PET data were acquired immediately after bolus intravenous injection of FDG ( $203 \pm 30$  MBq; fasting blood glucose =  $5.1 \pm 0.8$  mmol/L). PET data from 30 to 45 min were reconstructed to one image volume ( $344 \times 344 \times 127$  matrix) using Siemens e7 tools and an iterative algorithm (ordered subset expectation maximization with point-spread function model; 3 iterations, 21 subsets, 3D Gaussian filter with a full-width-half-maximum (FWHM) of 2 mm and zoom factor of 2.5). Scatter, decay and dead-time corrections were applied while attenuation correction was performed using the vendor-provided ultra-short echo time (UTE) sequence. Attenuation maps were generated using the RESOLUTE (Ladefoged et al., 2015) approach. The spatial

resolution of the reconstructed PET data was 4.75 mm along each direction.

A pseudo-continuous ASL (pCASL) sequence with a single-shot 3D gradient-and-spin-echo (3D GRASE) readout (Günther et al., 2005) was acquired within 10 min of FDG injection using the following parameters: TR/TE = 3500/22.76 ms, post-labelling delay (PLD) = 1.5 s, 64 label and control pairs, 26 contiguous slices (23 acquired slices with 15.4% oversampling and 6/8 Partial Fourier in the slice-encoding direction; parallel imaging acceleration factor of 2 along the phase-encoding direction, with GRAPPA reconstruction, and refocusing flip angle of 180 degrees), bandwidth = 2004 Hz/pixel, and  $3.8 \times 3.8 \times 6 \text{ mm}^3$  voxel size. The labelling consisted of a 1.5 s train of RF pulses positioned approximately 9 cm below the center (anterior commissure-posterior commissure, AC-PC) of the imaging plane and included two nonselective inversion pulses for suppression of static background signal. Total acquisition time was 7.32 min. For CBF quantification, two calibration images were acquired; a proton density (M0) image using the ASL sequence minus label and background suppression RF pulses and TR of 5 s, and a phase-contrast velocity image for estimation of labelling efficiency (Aslan et al., 2010). Participants were instructed to keep their eyes closed for the first 30 min of the PET/MRI scan which encompassed the recommended PET uptake window and ASL scans. Finally, 3D T1-weighted anatomical images (1 mm<sup>3</sup> isotropic resolution) were acquired with a 3D magnetization-prepared rapid gradient-echo sequence for evaluation of structural abnormalities, partial volume correction, and spatial normalization.

### 2.3. Image postprocessing

Image analyses were performed using SPM8 (<http://www.fil.ion.ucl.ac.uk>) and in-house MATLAB (2012a, The MathWorks, Natick, MA) scripts. ASL images were aligned to the first volume to correct for frame-to-frame head movement after manual alignment to AC-PC orientation. The aligned images were pair-wise subtracted and global signal spikes were removed prior to time averaging (see Supplementary Fig. A1 for further details). Prior to pair-wise subtraction, the ASL time series and structural (T1) image volume were registered to the M0 using the mean of the ASL time series as an intermediate. Grey matter (GM) and white matter (WM) masks were generated from T1 tissue segmentation using the MALPEM algorithm (Ledig et al., 2015) – a multi-atlas segmentation approach insensitive to pathology. The masks were downsampled to match ASL voxel size and transformed to a single partial volume (PV) mask, where  $PV = GM + 0.4 * WM$ , assuming WM contributes ~40% to total CBF (Du et al., 2006). The PV mask was applied to the perfusion-weighted images (i.e., mean ASL difference scaled by M0) to compensate for partial volume effects. A CBF map was then generated by transforming voxels in the perfusion-weighted image to CBF using a single-compartment model (Alsop et al., 2015) and labelling efficiency values estimated from phase-contrast imaging. The ASL-CBF images were then spatially transformed to the Montreal Neurological Institute (MNI) standard space using the unified segmentation-based normalization approach in SPM (Ashburner and Friston, 2005) and smoothed using a 10-mm FWHM Gaussian kernel. Similarly, the reconstructed PET images were corrected for PV using masks downsampled to match PET voxel size, spatially transformed and smoothed using the same methods. To match the spatial resolution of ASL to FDG-PET, CBF and FDG-PET images were convolved with a Gaussian function of FWHM of 10 mm, resulting in smoothed images with similar resolution: 11.7 and 10.7 mm in the slice and in-plane dimensions, respectively for ASL and 11.1 mm isotropic for FDG-PET (including the prior 2 mm post-reconstruction smoothing). Note that the resulting FWHM was estimated assuming the initial image resolution and kernel size of the Gaussian smoothing filter add in quadrature. To minimize inter-subject variability and permit direct comparison between modalities, the smoothed CBF and FDG-PET images were intensity normalized to their respective mean cerebellum GM value.

Because of differences in global mean GM CBF between patients and controls ( $t = -1.97, p = 0.06$ ), this reference region was used instead of global normalization, to prevent artificial inflation of regional CBF in the patient group in areas where perfusion is otherwise normal (Borghammer et al., 2008, 2009). The final relative ASL-CBF (rCBF) and FDG-PET (rCMRglc) images were used for group and single-subject analyses.

### 2.4. Qualitative visual analysis

PET and T1 images of all participants were evaluated in tandem by an experienced (30 years) dual board-certified physician in radiology and nuclear medicine (WP) to verify that PET images acquired using the PET/MRI were of optimal diagnostic quality. Visual inspections and evaluations were performed using Siemens *syngo*.via (Siemens Healthineers, Erlangen, Germany) clinical applications software.

Three trained readers with experience in PET and MRI visually inspected and rated each rCBF and rCMRglc image in a blinded manner; that is, each reader evaluated a total of 40 images unaware of diagnosis or imaging modality. Readers included a board-certified nuclear medicine physician (JCW) with 14 years of practice experience, a board-certified neurologist (EF) with 17 years of practice experience and expertise in applications of MRI and PET to studies of dementia, and a 5th year radiology resident (BYMK) trained in PET imaging and familiar with ASL. Readers were familiar with common imaging artefacts particularly signal loss artefacts related to PET signal attenuation or watershed artefacts in ASL, identified as bilateral signal dropout at border zones of adjacent arterial territories (Zaharchuk et al., 2009). Readers were instructed to rate overall image quality on a scale from 1 (insufficient) to 4 (excellent) based on impressions on image smoothness, noise, resolution, sharpness of contours and perceived contrast-to-noise. Presence of image artefacts was scored as either considerable (1), slight (2), or none (3). Readers were also encouraged to provide open-ended descriptions of perceived image artefacts. Image quality and artefacts were compared between modalities using the Wilcoxon signed rank test.

A forced-decision diagnosis between FTD or control was made after evaluating patterns of decreased activity in the following regions: right and left frontal, temporal, parietal, insular, anterior and posterior cingulate, thalamus and occipital, using evaluations methods described in Musiek et al. (2012). Each region was rated on a 4-point scale as either normal (4), mildly decreased (3), moderately decreased (2), or severely decreased (1). Images were read by scrolling through three orthogonal planes using FslView (<https://fsl.fmrib.ox.ac.uk>) with a fixed colour lookup table and fixed window/level settings. Measures of diagnostic accuracy – sensitivity, specificity, negative predictive value (NPV) and positive predictive value (PPV) – were calculated for each individual reader and averaged within each modality. These measures were calculated by computing the proportion of ratings with correct diagnosis, as confirmed by the radiology report. Differences in diagnostic accuracy between modalities were tested using a one-sided paired *t*-test to assess if ASL-CBF performed worse than FDG-PET. Concordance among readers was measured using Randolph's free-marginal multirater kappa ([justusrandolph.net/kappa/](http://justusrandolph.net/kappa/)), where a value  $\geq 0.70$  indicates adequate agreement. Because diagnostic accuracy and interrater agreement of FDG-PET in differential diagnosis of FTD are not significantly different when quantitative image analysis is augmented with visual reading compared to visual reading alone (Foster et al., 2007), stereotactic surface projections and *t/z*-score map were not presented to readers and were excluded from qualitative assessments.

### 2.5. Quantitative image analysis

Areas of hypoperfusion and hypometabolism were identified from each patient's rCBF and rCMRglc map, respectively, by comparing individual relative maps to the control group on a voxel-by-voxel basis

using the Crawford and Howell modified *t*-test (Crawford and Garthwaite, 2012) ( $t \leq -1.83, p < 0.05$ ) shown below:

$$t = \frac{X_{bvFTD} - \bar{X}_{HC}}{S_{HC} \sqrt{\left(\frac{n+1}{n}\right)}}$$

where,  $X_{bvFTD}$  represents a patient voxel value,  $\bar{X}_{HC}$  and  $S_{HC}$  are mean and standard deviation voxel values in controls, and  $n$  is the total number of controls. The Crawford and Howell modified *t*-test is better suited for deficit inference when a small control sample size is used, because it minimizes inflation of Type I errors and yields similar error rate for 10 or 100 control samples (Crawford and Garthwaite, 2012).

To test the extent of similarity between ASL-CBF and FDG-PET findings, a Jaccard similarity coefficient was calculated for each patient using *t*-score maps, where a Jaccard index closer to 1 demonstrates good agreement between modalities.

### 2.6. Group-level comparisons

To replicate and verify previous ASL-CBF and FDG-PET comparisons in FTD, most of which were performed at a group level, we compared mean grey matter rCBF to rCMRglc in 13 a priori regions of interest (ROIs) (cf. Fig. 1), which were created using the AAL atlas (Tzourio-Mazoyer et al., 2002), as implemented in SPM8. To minimize potential confounds from watershed artefacts in ASL, ROI masks were eroded around watershed areas. An independent samples *t*-test and Pearson correlation were performed to investigate regional differences between patient and control groups, and associations of ASL-CBF to FDG-PET across groups, respectively. The performance of ASL-CBF and FDG-PET in discriminating patients from controls was evaluated by receiver operator characteristics (ROC) analysis, to obtain sensitivity, specificity and areas under ROC curve (AUC) measures.

### 3. Results

PET/MRI scans were completed for all participants. A data set from one patient with possible bvFTD was removed due to corrupted list-mode files, which prevented retrospective PET reconstruction. Demographic and clinical characteristics of the participants are summarized in Table 1. Further clinical information for each of the patients including results from autopsy and genetic follow up where available, are presented in Table A1 of Supplementary material. Visual inspection and evaluation of PET and T1 images matched clinical diagnosis in all participants except the possible bvFTD patient, whose PET and T1 images were reported as normal.

#### 3.1. Qualitative evaluation

Representative rCBF and rCMRglc maps are displayed in Fig. 2. Compared to rCMRglc maps, rCBF maps had lower reported image quality ( $z = -4.77, p < 0.0001$ ) and more image artefacts

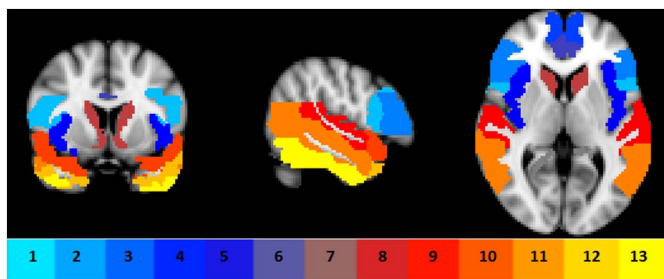


Fig. 1. A priori regions of interest (ROIs) masks overlaid on a single subject T1 image. ROIs comprised of frontal sub-regions (1–4), insula (5), anterior cingulate (6), precuneus (7), caudate (8) and temporal sub-regions (9–13) bilaterally.

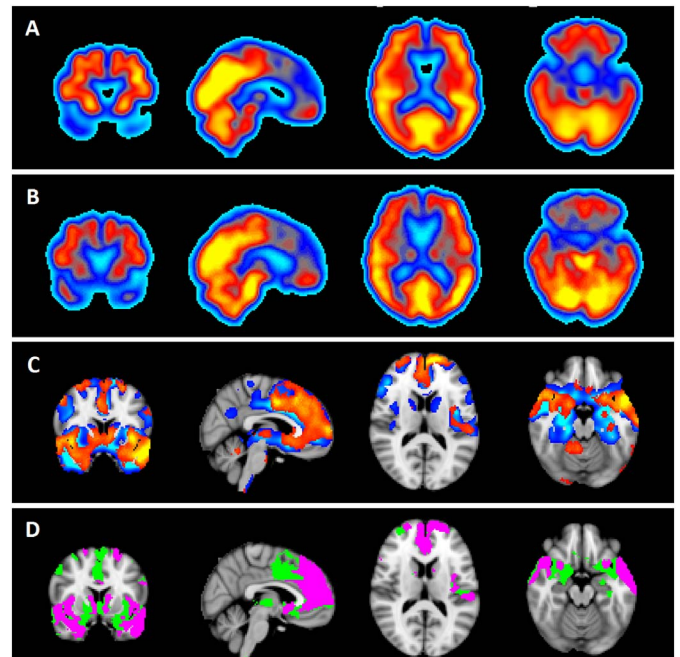


Fig. 2. Patient #2, rCMRglc (A) and rCBF (B) maps, illustrating images reviewed by readers. Slices in coronal, sagittal and axial are shown to highlight the potential of both modalities to yield similar diagnosis. All readers chose bvFTD diagnosis after reviewing either A or B images. (C) *t*-maps of voxelwise differences between patient and control group indicate areas of lower CBF (red-yellow) and less FDG uptake (blue-green). A large area overlapping hypometabolic and hypoperfusion regions can be seen in (D; green) with measured Jaccard index of 0.41. Restricting the concordance to a priori ROIs (purple) improved the Jaccard index to 0.60. Images are displayed in radiological convention.

( $z = -4.73, p < 0.0001$ ). Median rating scores of image quality and artefacts were 3.00 and 2.00 for rCBF compared to 4.00 and 3.00 for rCMRglc. Further details on image quality and artefact scores are described in the Supplementary material.

Concordance between clinical diagnosis and each reader's forced-diagnosis ranged from 83.30% to 94.40% for FDG-PET and 66.70 to 72.22% for ASL-CBF, excluding evaluations in the possible bvFTD patient. The overall agreement among readers for diagnosis was 80% for FDG-PET and 60% for ASL-CBF. The corresponding kappa coefficients for interrater reliability were 0.61 and 0.20 for FDG-PET and ASL-CBF, respectively. Agreement among readers was also estimated in disease-related brain regions to determine if readers can detect similar disease patterns between modalities (Table 2). Overall agreement and kappa coefficients were higher for FDG-PET in all regions except in the temporal cortices. Measures of diagnostic accuracy averaged across readers were also significantly higher for FDG-PET compared to ASL-CBF and are summarized in Fig. 3.

#### 3.2. Quantitative assessments

In all patients, areas of hypometabolism were more expansive than hypoperfused areas. An example of *t*-score maps representing areas of hypoperfusion and hypometabolism in one patient is shown in Fig. 2C. Corresponding concordance maps signifying extent of overlap between *t*-score maps are shown in Fig. 2D. Individual *t*-scores and concordance maps for all patients are shown in the Supplementary material. Individual Jaccard similarity indices quantifying extent of concordance are listed in Table 3, as well as overall percent agreement from qualitative assessments.

#### 3.3. Between-subjects group comparisons

Lower rCMRglc was observed bilaterally in all ROIs in the patient

**Table 2**  
Qualitative and quantitative regional assessments of diagnostic performance between modalities.

Region	Modality	Pearson <i>r</i>	AUC*	Sensitivity	Specificity	Overall agreement (%)	Kappa
Frontal	FDG-PET	0.74	0.89	0.8	1	71	0.62
	ASL-CBF		0.78	0.7	0.7	40	0.20
Temporal	FDG-PET	0.42	0.78	0.7	0.9	24	-0.02
	ASL-CBF		0.66	0.6	0.7	33	0.11
Insula	FDG-PET	0.57	0.86	0.8	0.6	79	0.72
	ASL-CBF		0.65	0.7	0.5	56	0.40
ACC	FDG-PET	0.71	0.85	0.7	0.8	52	0.36
	ASL-CBF		0.76	0.7	0.8	39	0.19
All ROIs	FDG-PET	0.68	0.87	0.8	0.7	71	0.62
	ASL-CBF		0.75	0.8	0.6	52	0.36

\* All regions reached statistically significant difference between modalities at  $p < 0.05$ .

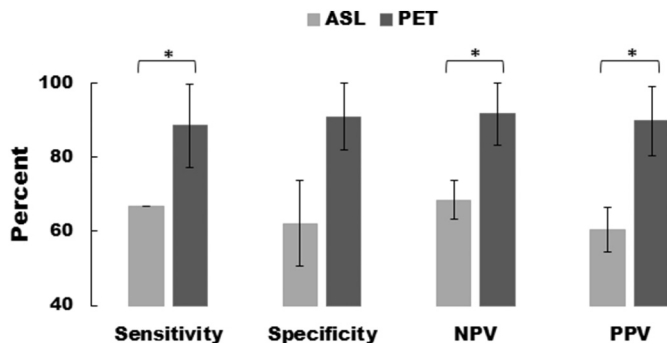


**Fig. 3.** A comparison of measures of diagnostic performance between ASL-CBF and FDG-PET from visual assessments. Significant difference between modalities are indicated by \* ( $p < 0.05$ ). Error bars correspond to standard deviation. NPV and PPV are the negative and positive predictive value.

group compared to controls, except in the left temporal regions, while decreased rCBF was found in the patient group in 13 of the 26 ROIs (Fig. 4). Of note, the magnitude of the rCMRglc difference between patients and controls was greater than the corresponding rCBF difference in all regions. Both modalities revealed greater magnitude of *t*-values in right side regions compared to left side regions (cf. Table A2 of Supplementary material for outline of *t*-values from all regions). Pearson correlation analysis revealed a strong correlation between modalities across all ROIs ( $r = 0.68, p < 0.001$ ) (Fig. 5). A Bland-Altman assessment indicated minimal bias between modalities (Fig. 5), suggesting that ASL-CBF provided similar regional brain measures as FDG-PET. Similarly, moderate-to-strong correlations between modalities were also observed in brain regions commonly associated with bvFTD, as shown in Fig. 6 (correlation coefficients are listed in Table 2). These observations were further confirmed using dot plots (Fig. 6) that demonstrated similar patterns of regional mean distributions in patients and controls for both modalities. When diagnostic performance was

**Table 3**  
Summary of individual patient demographics and results from between modalities concordance measures.

Patient #	Diagnosis	Age (years)	Gender	Years of illness	Jaccard Index	Agreement among readers	
						FDG-PET	ASL-CBF
1	Probable bvFTD	79	M	5	0.043	3/3	3/3
2	Probable bvFTD	68	M	8	0.41	3/3	3/3
3	Probable bvFTD	74	F	9	0.045	2/3	2/3
4	Probable svPPA	58	F	6	0.19	3/3	2/3
5	Possible bvFTD	73	M	2	0.03	3/3	3/3
6	Probable bvFTD	54	F	4	0.71	3/3	3/3
7	Probable bvFTD	73	M	7	0.36	2/3	2/3
8	Probable bvFTD	62	M	6	0.44	3/3	3/3
9	Probable bvFTD + nPPA	67	F	1	0.36	3/3	2/3
10	Probable bvFTD	55	F	5	0.44	3/3	2/3

compared, higher sensitivity, specificity and AUC were found for FDG-PET compared to ASL-CBF (Table 2). Results of unilateral regional performance and regional correlation between modalities are outlined in Table A2 of Supplementary material.

#### 4. Discussion

This study exploited gains in temporal and spatial registration offered by hybrid PET/MRI to assess the use of ASL as a suitable alternative to FDG-PET in diagnosing FTD, as proposed by recent studies (Du et al., 2006; Fällmar et al., 2017; Steketee et al., 2015; Tosun et al., 2016; Weyts et al., 2017). To provide a comprehensive evaluation of the diagnostic performance of ASL compared to FDG-PET, we used established qualitative and quantitative metrics of diagnostic equivalency, and evaluated images on individual- and grouped-level basis. This approach revealed strong evidence for the potential of ASL to detect similar spatial patterns of abnormalities as FDG-PET in individuals with FTD. However, the sensitivity and specificity of ASL in differentiating a patient from healthy older individuals was not as high as that of FDG-PET.

In clinics, in the absence of definite diagnosis from histopathology, diagnosis of probable FTD can be made using neuroimaging, in accordance with international consensus criteria. Findings of frontal and/or temporal atrophy on MRI or CT, hypometabolism on FDG-PET or hypoperfusion on SPECT, with relative integrity of posterior brain regions, signifies probable bvFTD (Rascovsky et al., 2011). The clinical significance of FDG-PET has been validated in pathologically confirmed FTD and AD patients, where visual assessments of FDG-PET images were found to be highly specific and sensitive in differentiating FTD from AD (Foster et al., 2007). When FDG-PET is combined with neurological assessments and neuropsychological testing (Foster et al., 2007; Mendez et al., 2007) or added to GM atrophy detected by MRI (Dukart et al., 2011; Kawachi et al., 2006), diagnostic accuracy and confidence in detecting FTD is further increased. SPECT, on the other hand, can be used in lieu of PET, as SPECT can also improve clinical

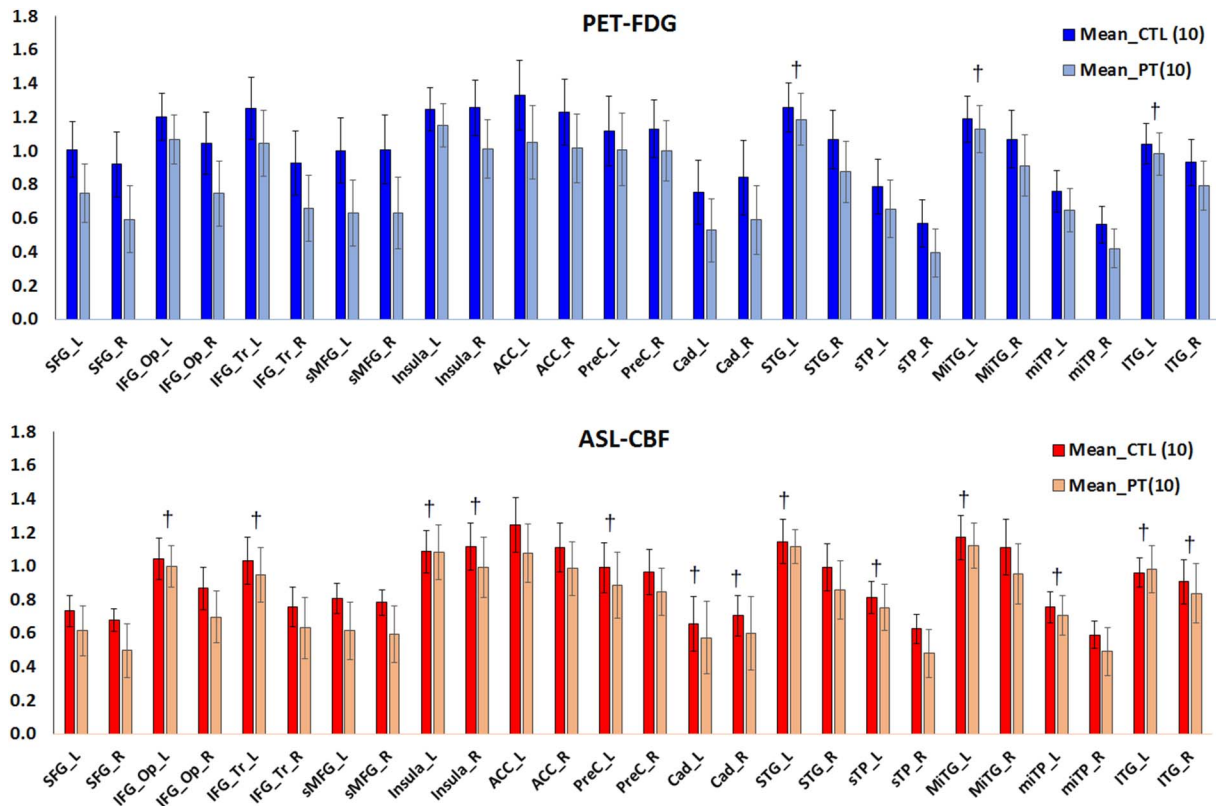


Fig. 4. Regional grouped means of glucose uptake (top) and cerebral blood flow (bottom). Errors bars indicate standard deviation. Significant difference between groups was seen in all regions except † where  $p > 0.05$ . CTL = control subjects, PT = FTD patients.

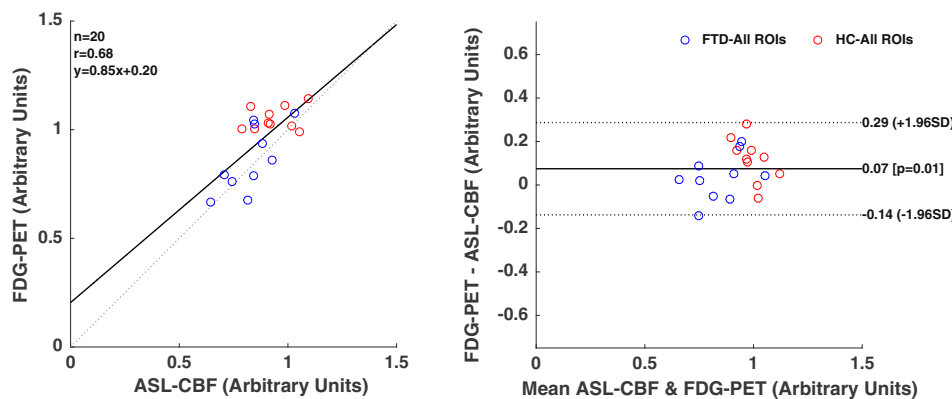


Fig. 5. Association between ASL-CBF and FDG-PET across all regions of interests. A strong correlation between modalities can be seen in regression plot ( $p < 0.001$ ) (left) and the Bland-Altman plot (right) reveals close agreement between modalities with slight systematic bias possibly due to relatively poor SNR of the ASL signal ( $-0.14$  to  $0.29$ ,  $r = 0.07$ ,  $p = 0.01$ ). HC = control subjects.

diagnosis of FTD (McNeill et al., 2006), but with lower sensitivity (Yeo et al., 2013). ASL is comparable to SPECT perfusion imaging (Liu et al., 2012) and has been shown to produce similar regional patterns of hypoperfusion in patients with dementia (Du et al., 2006; Hu et al., 2010). However, the higher spatial resolution of ASL — nearly twice that of SPECT, and the potential for technetium-based SPECT perfusion tracers to overestimate CBF in low flow regions (Catafau, 2001), makes ASL a better alternative for clinical diagnosis of FTD, especially given that ASL can be acquired along with anatomical MRI in the same scan session.

Efforts have been made to ready ASL for clinical adoption, including recommendations for standard imaging parameters (Alsop et al., 2015), guidelines on image interpretation for neuroradiologists (Grade et al., 2015), and multi-vendor trials demonstrating similarity among scanner manufacturers (Mutsaerts et al., 2015). However, clinical adoption of ASL as part of a diagnostic workup for FTD has been restrained by

inconclusive evidence from previous investigations, which are relatively recent and as such scarce. Qualitative assessments of visual impressions performed recently by Fällmar et al. (2017) found higher specificity, PPV and inter-rater agreement when ASL is used to discriminate bvFTD, semantic dementia and AD patients from controls, compared to FDG-PET. But in the same cohorts, FDG-PET produced higher sensitivity, NPV and accuracy compared to ASL. In contrast, we found that visual evaluations of FDG-PET images produced higher sensitivity, specificity, PPV and NPV compared to ASL. Inter-rater agreement was also higher for PET, meaning the FDG images were more reliable and easier to interpret by readers. Two other studies using subjective visual rating methods to compare the diagnostic performance of ASL and FDG-PET reported contrasting findings; 1) higher diagnostic accuracy with FDG-PET in dementia (AD + FTD) patients (Weys et al., 2017), 2) higher inter-rater agreement in FDG-PET in AD patients (Musiek et al., 2012), and 3) matched sensitivity and specificity for

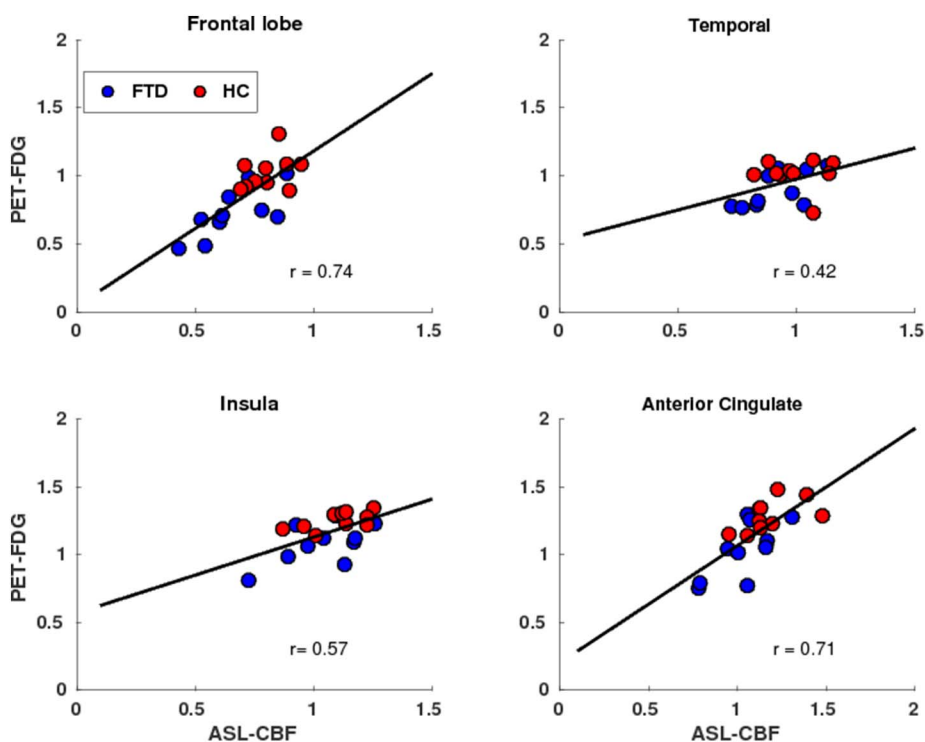
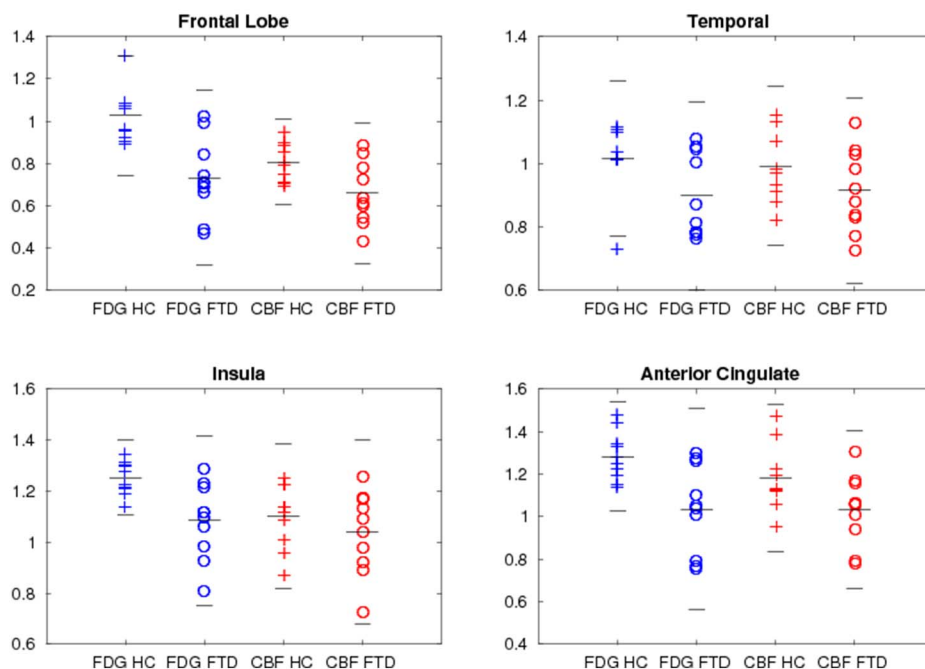


Fig. 6. Comparison between cerebral perfusion and glucose metabolism in key regions across both groups. Moderate-to-strong correlation between perfusion and metabolism can be seen in all regions (top panel), and significant differences ( $p < 0.05$ ) between patients and controls (bottom panel) were found in all regions for FDG-PET and in the frontal lobe and anterior cingulate for ASL-CBF. Line plots of mean, and 95% confidence intervals for the mean are included in dot plots.



differentiating AD from normal aging (Musiek et al., 2012). Since our study measured diagnostic performance of ASL and FDG-PET solely in FTD patients, but not in other dementias, reconciling our findings with these prior studies is challenging. In Weyts et al. (2017), three of the nine patients were clinically diagnosed as FTD, and in all three cases, forced diagnosis following visual assessments of FDG-PET images by nuclear medicine physicians matched clinical diagnosis, while ASL readings performed by separate readers (neuroradiologists) correctly identified one of the three FTD patients. In Fällmar et al. (2017), subjective visual assessments were made on individual statistical (z-score)

maps and not directly on FDG or CBF images. In addition, the sensitivity, specificity and inter-rater agreement were not specified for the bvFTD cases separately, rather the authors noted that FDG-PET readings compared to ASL, yielded higher rate for correct classification of FTD cases as patient scans (Fällmar et al., 2017). It is quite possible that the diagnostic performance and inter-rater agreement of ASL in our study could have been improved if individual statistical maps were included to augment subjective visual interpretations (Kemp et al., 2005). Although for FDG-PET, diagnosis of dementia based solely on subjective visual interpretations are equally accurate as diagnosis made

with inclusion of individual statistical maps (Foster et al., 2007). Perhaps, with increased reader training, ASL can achieve robust visual assessment accuracy similar to FDG-PET.

Findings from our quantitative assessments using ROI analysis at the group-level and estimations of concordance between individual hypoperfusion and hypometabolic regions, supported our qualitative findings. Foremost, areas of decreased glucose metabolism identified in individual statistical maps extended beyond areas of reduced perfusion in all patients. Likewise, examination of between-group differences from ROIs, showed greater magnitude of deficit, as well as greater number of areas with significantly decreased activity for FDG-PET compared to ASL. Across all regions, we found higher specificity and overall diagnostic accuracy (AUC) in discriminating patients from controls for FDG-PET, while sensitivity was matched between modalities. This is consistent with a prior study, which found similar sensitivity, higher specificity and slightly higher AUC for FDG-PET compared to ASL in 32 bvFTD patients and 15 cognitively normal controls (Tosun et al., 2016). Taken together, these findings reinforce impressions from visual assessments of higher FDG-PET diagnostic performance compared to ASL. Nonetheless, ASL has the potential to provide comparable diagnostic information as FDG-PET in FTD, since ASL and FDG-PET are known to be closely matched in healthy (Anazodo et al., 2015; Cha et al., 2013) and AD (Musiek et al., 2012; Vercllytte et al., 2015) brains, and as we demonstrated here using Pearson correlations in FTD brains as well. This association is well illustrated in the possible bvFTD case, where initial diagnosis prior to PET/MRI was revised following negative findings on FDG-PET and anatomical MRI. In this patient, ASL could have been substituted for FDG-PET, because visual reviews of rCBF images resulted in the same unanimous negative finding as reviews of rCMRglc. Perhaps, the clinical role of ASL in FTD diagnosis could be an adjunct to anatomical MRI in early-stages of FTD, where ASL acquired in the same session as anatomical MRI can be used to rule out normal aging or other dementias, reserving FDG-PET for cases where MRI is equivocal (Fällmar et al., 2017).

It is unclear if ASL provides added clinical value to FTD diagnosis beyond what can be achieved with anatomical MRI alone. An earlier study found that adding ASL to anatomical MRI improved differentiation of FTD from normal aging and AD (Du et al., 2006). However, more recent studies have shown that ASL offers little or no added diagnostic value to anatomical MRI in FTD diagnosis (Bron et al., 2014, 2016), rather areas of GM loss tend to exceed areas of decreased perfusion (Steketee et al., 2015; Zhang et al., 2011). Establishing a consensus on clinical utility of ASL in diagnosis of FTD from prior studies is limited by heterogeneity in ASL techniques, diversity of study populations such as mixed FTD subtypes, use of relatively small sample sizes, and differences in image analysis methodology. For instance, eight studies within the last decade which investigated diagnostic accuracy of ASL in comparison to FDG-PET or anatomical MRI, employed five different label and readout scheme pairs along with varying PLD (1 to 2 s) (Bron et al., 2014, 2016; Du et al., 2006; Fällmar et al., 2017; Steketee et al., 2015; Tosun et al., 2016; Weyts et al., 2017; Zhang et al., 2011). Choice of ASL techniques (label scheme, readout sequences, PLD) can significantly impact the signal-to-noise ratio (SNR), lead to image artefacts such as watershed and motion, and alter perceived contrast (grey-to-white matter ratio) (Alsop et al., 2015; Grade et al., 2015). Even with the use of the recommended label scheme, pCASL can still produce significant differences in global blood flow, temporal and spatial SNR, and GM-WM ratio when paired with different readout sequences (Vidorreta et al., 2013). In this study, we used a pCASL labelling scheme and one of the recommended readout sequences (3D-GRASE), in order to minimize motion artefacts and maximize temporal SNR and GM-WM contrast ratio (Vidorreta et al., 2013). However, our choice of PLD was implemented prior to publication of the ASL whitepaper, and is shorter than the recommended 2 s for imaging older brains. The PLD used in this study is common in FTD studies (Bron et al., 2014, 2016; Verfaillie et al., 2015; Weyts et al., 2017), where often the decision was made in

an effort to maximize ASL signal while minimizing potential watershed artefacts caused by image acquisition prior to labelled blood-water arrival. Clearly, in our study watershed artefacts significantly impacted ASL image quality and may have subsequently contributed to the lower diagnostic performance measured in ASL. However, diagnostic accuracy from quantitative measurements was restricted to regions outside the watershed zone and as such ASL poorer performance cannot be attributed solely to this artefact. Image artefacts were also reported for FDG-PET, mostly related to temporal lobe signal attenuation. Areas of the brain around the base of the skull and mastoid process can have up to ~5% error in PET signal attenuation because MR-based attenuation correction methods can have difficulty resolving bone from mixed air/tissue/bone voxels (Ladefoged et al., 2015). In such cases inclusion of attenuation correction maps, standard in clinical practice, and free image windowing level may have helped resolve attenuation artefacts.

Despite perceived challenges in image quality, rCBF and rCMRglc images were sufficient in characterizing FTD in our cohort, revealing typical patterns of pathological asymmetry associated with FTD. First, frontal hypometabolism and hypoperfusion were observed in patients compared to controls, in line with previous studies (Du et al., 2006; Foster et al., 2007; Ishii et al., 1998; Jeong et al., 2005) and in agreement with common clinical presentations of bvFTD, where impairment in executive function or working memory and behavioural symptoms such as disinhibition, apathy and impulsivity are observed earlier on, indicative of frontal lobe involvement (Weder et al., 2007). Second, the extent of temporal lobe hypometabolism was reduced compared to the frontal lobe and restricted to the temporal poles and right temporal cortex. Third, deficits in glucose metabolism and perfusion were greater in the right hemisphere in all regions surveyed, reflecting the known right-hemisphere lateralization in bvFTD. Finally, we observed bilateral hypometabolism in additional regions associated with FTD pathology including the frontoinsula, anterior cingulate, precuneus, and caudate regions (Schroeter et al., 2014). In general, the clinical and anatomical presentations in our cohort (~63% right hemisphere predominant atrophy and 67% frontal predominant bvFTD) were well represented by functional changes observed by FDG-PET and ASL.

The apparent mismatch in diagnostic performance between ASL and FDG-PET described in this study may be a result of the small sample size used. Two studies with twice the number of bvFTD patients found that ASL had comparable diagnostic information to FDG-PET (Tosun et al., 2016) and improved disease classification when added to anatomical MRI (Du et al., 2006). However, these studies evaluated ASL in groups of patients and controls. The heterogeneity of FTD, in terms of genetic, pathology and clinical manifestations stresses the need for more studies to examine the clinical utility of ASL on an individual level rather than at the group level. Differences in the point-spread function (PSF) of ASL and FDG-PET images may have contributed to the apparent mismatch in diagnostic performance between modalities. This confound was minimized by applying comparable spatial smoothing to both the CBF (10 mm FWHM) and FDG-PET (2 + 10 mm FWHM) images, and by including partial volume correction using spatial priors downsampled to each modality's voxel size. The spatial smoothing applied to the CBF images could have amplified the inherent blurring of GRASE-ASL images in the slice direction (Vidorreta et al., 2013), increasing the effective PSF of CBF relative to FDG-PET. However, reducing the spatial smoothing filter to compensate for this effect, would reduce the SNR and further minimize the sensitivity of ASL to detect regional abnormalities. Because ASL is inherently sensitive to motion and susceptibility distortion artefacts, which further minimizes the already low SNR and significantly impacts sensitivity, future studies will need to employ advanced image processing techniques beyond those implemented in this study, such as spatio-temporal denoising techniques (Spann et al., 2017) and geometric distortion correction strategies (Gelman et al., 2014; Madai et al., 2016). The sensitivity of ASL could have improved using higher-phased array receiver coils such as 32/64 channel head coils which offer up to twice the SNR of standard — 8/12

channel coils. Similar to our study, all previous studies (Bron et al., 2014, 2016; Du et al., 2006; Fällmar et al., 2017; Steketee et al., 2015; Tosun et al., 2016; Verfaillie et al., 2015; Zhang et al., 2011) where the diagnostic performance of ASL was explored in patients with FTD in comparison to FDG-PET or anatomical MRI, used a standard receiver coil. The use of higher-phased array receiver coil to improve the SNR of ASL could likely improve the sensitivity of the technique and hence the agreement with FDG-PET. It is possible that ASL is less sensitive than FDG-PET in differentiating FTD from normal aging because unlike AD which is associated with vascular dysfunction and as such can be detected well with ASL even in prodromal stages (Iturria-Medina et al., 2016), FTD has no known vascular pathophysiology. Given the growing prevalence of PET/MRI, large multi-center studies where ASL imaging techniques are standardized can be performed using methodologies outlined in this study, to better understand the potential clinical role of ASL in FTD diagnosis and management.

## Acknowledgement

The authors would like to thank Ms. Julia MacKinley and Ms. Kristy Coleman for assistance with participant recruitment and Mr. John Butler and Mrs. Heather Biernaski for assistance with PET/MR imaging.

## Funding sources

This study was funded in part by a Schulich School of Medicine and Dentistry Dean's Initiative Research Grant (Elizabeth Finger; R4273A09), the Canadian Institutes of Health Research (Keith S St Lawrence; PJT-148600), and in-kind support from London X-ray Associates, London, Ontario. The hybrid PET/MRI system was funded primarily from a Canadian Foundation for Innovation Grant.

## Conflicts of interest

Matthias Günther receives support and development funds from Siemens Healthcare. All other authors have no conflicts of interest to declare.

## Appendix A. Supplementary data

Supplementary data to this article can be found online at <https://doi.org/10.1016/j.nicl.2017.10.033>.

## References

- Albert, M., DeCarli, C.S., DeKosky, S.T., de Leon, M.J., Foster, N.L., Fox, N.C., Frank, R., Frackowiak, R.S., Jack, C.R., Jagust, W.J., Knopman, D.S., Morris, J.C., Petersen, R.C., Reiman, E., Scheltens, P., Small, G., Soininen, H., Thal, L., Wahlund, L.-O., Thies, W., Weiner, M., Khachaturian, Z., 2005. The use of MRI and PET for clinical diagnosis of dementia and investigation of cognitive impairment: a consensus report. *Alzheimer's Assoc. Neuroimaging Work Gr. Consens. Rep.* 1–15.
- Alsop, D.C., Detre, J.A., Golay, X., Günther, M., Hendrikse, J., Hernandez-Garcia, L., Lu, H., MacIntosh, B.J., Parkes, L.M., Smits, M., van Osch, M.J.P., Wang, D.J.J., Wong, E.C., Zaharchuk, G., 2015. Recommended implementation of arterial spin-labeled perfusion MRI for clinical applications: a consensus of the ISMRM perfusion study group and the European consortium for ASL in dementia. *Magn. Reson. Med.* 73, 102–116. doi:<https://doi.org/10.1002/mrm.25197>.
- Anazodo, U.C., Thiessen, J.D., Ssali, T., Mandel, J., Günther, M., Butler, J., Pavlosky, W., Prato, F.S., Thompson, R.T., St. Lawrence, K.S., 2015. Feasibility of simultaneous whole-brain imaging on an integrated PET-MRI system using an enhanced 2-point Dixon attenuation correction method. *Front. Neurosci.* 8, 1–11. <http://dx.doi.org/10.3389/fnins.2014.00434>.
- Ashburner, J., Friston, K.J., 2005. Unified segmentation. *NeuroImage* 26, 839–851. <http://dx.doi.org/10.1016/j.neuroimage.2005.02.018>.
- Aslan, S., Xu, F., Wang, P.L., Uh, J., Yezhuvath, U.S., van Osch, M., Lu, H., 2010. Estimation of labeling efficiency in pseudocontinuous arterial spin labeling. *Magn. Reson. Med.* 63, 765–771. doi:<https://doi.org/10.1002/mrm.22245>.
- Binnewijzend, M.A., Kuijter, J.P., Benedictus, M.R., der van Flier, W.M., Wink, M.A., Wattjes, M.P., van Berckel, B.N.M., Scheltens, P., Barkhof, F., 2013. Cerebral blood flow measured arterial spin-labeling MR imaging in Alzheimer disease and mild cognitive impairment. *Radiology* 267, 221–230.
- Borghammer, P., Jonsdottir, K.Y., Cumming, P., Ostergaard, K., Vang, K., Ashkanian, M., Vafaee, M., Iversen, P., Gjedde, A., 2008. Normalization in PET group comparison studies—the importance of a valid reference region. *NeuroImage* 40, 529–540. <http://dx.doi.org/10.1016/j.neuroimage.2007.12.057>.
- Borghammer, P., Cumming, P., Aanerud, J., Gjedde, A., 2009. Artefactual subcortical hyperperfusion in PET studies normalized to global mean: lessons from Parkinson's disease. *NeuroImage* 45, 249–257. <http://dx.doi.org/10.1016/j.neuroimage.2008.07.042>.
- Bron, E.E., Steketee, R.M.E., Houston, G.C., Oliver, R.A., Achterberg, H.C., Loog, M., van Swieten, J.C., Hammers, A., Niessen, W.J., Smits, M., Klein, S., 2014. Diagnostic classification of arterial spin labeling and structural MRI in presenile early stage dementia. *Hum. Brain Mapp.* 35, 4916–4931. <http://dx.doi.org/10.1002/hbm.22522>.
- Bron, E.E., Smits, M., Pappa, J.M., Steketee, R.M.E., Meijboom, R., de Groot, M., van Swieten, J.C., Niessen, W.J., Klein, S., 2016. Multiparametric computer-aided differential diagnosis of Alzheimer's disease and frontotemporal dementia using structural and advanced MRI. *Eur. Radiol.* 1–11. <http://dx.doi.org/10.1007/s00330-016-4691-x>.
- Catafau, A.M., 2001. *Brain SPECT in clinical practice. Part I: perfusion.* *J. Nucl. Med.* 42, 259–271.
- Centers for Medicare & Medicaid Services, 2009. *National Coverage Determination (NCD) for FDG PET for Dementia and Neurodegenerative Diseases.* (220.6.13).
- Cha, Y.-H.K., Jog, M.A., Kim, Y.-C., Chakrapani, S., Kraman, S.M., Wang, D.J., 2013. Regional correlation between resting state FDG PET and pCASL perfusion MRI. *J. Cereb. Blood Flow Metab.* 33, 1909–1914. <http://dx.doi.org/10.1038/jcbfm.2013.147>.
- Coleman, K.K.L., Coleman, B.L., MacKinley, J.D., Pasternak, S.H., Finger, E.C., 2017. Association between Montreal Cognitive Assessment sub-item scores and corresponding cognitive test performance in patients with frontotemporal dementia and related disorders. *Dement. Geriatr. Cogn. Disord.* 43, 170–179. <http://dx.doi.org/10.1159/000457119>.
- Crawford, J.R., Garthwaite, P.H., 2012. Single-case research in neuropsychology: a comparison of five forms of t-test for comparing a case to controls. *Cortex* 48, 1009–1016. <http://dx.doi.org/10.1016/j.cortex.2011.06.021>.
- Diehl-Schmid, J., Grimmer, T., Drzezga, A., Bornschein, S., Riemenschneider, M., Förstl, H., Schwaiger, M., Kurz, A., 2007. Decline of cerebral glucose metabolism in frontotemporal dementia: a longitudinal <sup>18</sup>F-FDG-PET-study. *Neurobiol. Aging* 28, 42–50. <http://dx.doi.org/10.1016/j.neurobiolaging.2005.11.002>.
- Du, A.T., Jahng, G.H., Hayasaka, S., Kramer, J.H., Rosen, H.J., Gorno-Tempini, M.L., Rankin, K.P., Miller, B.L., Weiner, M.W., Schuff, N., 2006. Hypoperfusion in frontotemporal dementia and Alzheimer disease by arterial spin labeling MRI. *Neurology* 67, 1215–1220. <http://dx.doi.org/10.1212/01.wnl.0000238163.71349.78>.
- Dukart, J., Mueller, K., Horstmann, A., Barthel, H., Möller, H.E., Villringer, A., Sabri, O., Schroeter, M.L., 2011. Combined evaluation of FDG-PET and MRI improves detection and differentiation of dementia. *PLoS One* 6, e18111. <http://dx.doi.org/10.1371/journal.pone.0018111>.
- Fällmar, D., Haller, S., Lilja, J., Danfors, T., Kilander, L., Tolboom, N., Egger, K., Kellner, E., Croon, P.M., Verfaillie, S.C.J., van Berckel, B.N.M., Ossenkoppele, R., Barkhof, F., Larsson, E.-M., 2017. Arterial spin labeling-based Z-maps have high specificity and positive predictive value for neurodegenerative dementia compared to FDG-PET. *Eur. Radiol.* <http://dx.doi.org/10.1007/s00330-017-4784-1>.
- Folstein, M.F., Folstein, S.E., McHugh, P.R., 1975. "Mini-mental state". A practical method for grading the cognitive state of patients for the clinician. *J. Psychiatr. Res.* 12, 189–198.
- Foster, N.L., Heidebrink, J.L., Clark, C.M., Jagust, W.J., Arnold, S.E., Barbas, N.R., DeCarli, C.S., Turner, R.S., Koeppe, R.A., Higdon, R., Minoshima, S., 2007. FDG-PET improves accuracy in distinguishing frontotemporal dementia and Alzheimer's disease. *Brain* 130, 2616–2635. <http://dx.doi.org/10.1093/brain/awn177>.
- Gelman, N., Silavi, A., Anazodo, U., 2014. A hybrid strategy for correcting geometric distortion in echo-planar images. *Magn. Reson. Imaging.* <http://dx.doi.org/10.1016/j.mri.2014.02.011>.
- Gorno-Tempini, M.L., Hillis, A.E., Weintraub, S., Kertesz, A., Mendez, M., Cappa, S.F., Ogar, J.M., Mohr, J.D., Black, S., Boeve, B.F., Manes, F., Dronkers, N.F., Vandenberghe, R., Rascovsky, K., Patterson, K., Miller, B.L., Knopman, D.S., Hodges, J.R., Mesulam, M.M., Grossman, M., 2011. Classification of primary progressive aphasia and its variants. *Neurology* 76, 1006–1014. <http://dx.doi.org/10.1212/WNL.0b013e31821103e6>.
- Grade, M., Hernandez Tamames, J.A., Pizzini, F.B., Achten, E., Golay, X., Smits, M., 2015. A neuroradiologist's guide to arterial spin labeling MRI in clinical practice. *Neuroradiology.* <http://dx.doi.org/10.1007/s00234-015-1571-z>.
- Günther, M., Oshio, K., Feinberg, D.A., 2005. Single-shot 3D imaging techniques improve arterial spin labeling perfusion measurements. *Magn. Reson. Med.* 54, 491–498. <http://dx.doi.org/10.1002/mrm.20580>.
- Hu, W.T., Wang, Z., Lee, V.M.-Y., Trojanowski, J.Q., Detre, J.A., Grossman, M., 2010. Distinct cerebral perfusion patterns in FTLD and AD. *Neurology* 75, 881–888. <http://dx.doi.org/10.1212/WNL.0b013e3181f1e35>.
- Ishii, K., Sakamoto, S., Sasaki, M., Kitagaki, H., Yamaji, S., Hashimoto, M., Imamura, T., 1998. Cerebral glucose metabolism in patients with frontotemporal dementia. *J. Nucl. Med.* 39, 1875–1878.
- Iturria-Medina, Y., Sotero, R.C., Toussaint, P.J., Mateos-Perez, J.M., Evans, A.C., T.A.D.N. Initiative, 2016. Early role of vascular dysregulation on late-onset Alzheimer's disease based on multifactorial data-driven analysis. *Nat. Commun.* 7, 11934. <http://dx.doi.org/10.1038/ncomms11934>.
- Jeong, Y., Cho, S.S., Park, J.M., Kang, S.J., Lee, J.S., 2005. PET findings in frontotemporal dementia: an SPM analysis of 29 patients. *J. Nucl. Med.* 46, 233–239.
- Kawachi, T., Ishii, K., Sakamoto, S., Sasaki, M., Mori, T., Yamashita, F., Matsuda, H., Mori, E., 2006. Comparison of the diagnostic performance of FDG-PET and VBM-MRI in

- very mild Alzheimer's disease. *Eur. J. Nucl. Med. Mol. Imaging* 33, 801–809. <http://dx.doi.org/10.1007/s00259-005-0050-x>.
- Kemp, P.M., Hoffmann, S.A., Holmes, C., Bolt, L., Ward, T., Holmes, R.B., Fleming, J.S., 2005. The contribution of statistical parametric mapping in the assessment of pre-cuneal and medial temporal lobe perfusion by 99mTc-HMPAO SPECT in mild Alzheimer's and Lewy body dementia. *Nucl. Med. Commun.* 26, 1099–1106. <http://dx.doi.org/10.1097/00006231-200512000-00009>.
- Ladefoged, C.N., Benoit, D., Law, I., Holm, S., Kjaer, A., Højgaard, L., Hansen, A.E., Andersen, F.L., 2015. Region specific optimization of continuous linear attenuation coefficients based on UTE (RESOLUTE): application to PET/MR brain imaging. *Phys. Med. Biol.* 60, 8047–8065. <http://dx.doi.org/10.1088/0031-9155/60/20/8047>.
- Ledig, C., Heckemann, R.A., Hammers, A., Lopez, J.C., Newcombe, V.F.J., Makropoulos, A., Lötjönen, J., Menon, D.K., Rueckert, D., 2015. Robust whole-brain segmentation: application to traumatic brain injury. *Med. Image Anal.* 21, 40–58. <http://dx.doi.org/10.1016/j.media.2014.12.003>.
- Liu, P., Uh, J., Devous, M.D., Adinoff, B., Lu, H., 2012. Comparison of relative cerebral blood flow maps using pseudo-continuous arterial spin labeling and single photon emission computed tomography. *NMR Biomed.* 25, 779–786. <http://dx.doi.org/10.1002/nbm.1792>.
- Madaï, V.I., Martin, S.Z., von Samson-Himmelstjerna, F.C., Herzig, C.X., Mutke, M.A., Wood, C.N., Thamm, T., Zweynert, S., Bauer, M., Hetzer, S., Günther, M., Sobesky, J., 2016. Correction for susceptibility distortions increases the performance of arterial spin labeling in patients with cerebrovascular disease. *J. Neuroimaging* 26, 436–444. doi:<https://doi.org/10.1111/jon.12331>.
- McNeill, R., Sare, G.M., Manoharan, M., Testa, H.J., Mann, D.M.A., Neary, D., Snowden, J.S., Varma, A.R., 2006. Accuracy of single-photon emission computed tomography in differentiating frontotemporal dementia from Alzheimer's disease. *J. Neurol. Neurosurg. Psychiatry* 78, 350–355. <http://dx.doi.org/10.1136/jnnp.2006.106054>.
- Mendez, M.F., Shapira, J.S., McMurtry, A., Licht, E., Miller, B.L., 2007. Accuracy of the clinical evaluation for frontotemporal dementia. *Arch. Neurol.* 64, 830. <http://dx.doi.org/10.1001/archneur.64.6.830>.
- Moodley, K.K., Perani, D., Minati, L., Anthony Della Rosa, P., Pennycook, F., Dickson, J.C., Barnes, A., Elisa Contarino, V., Michopoulou, S., D'Incerti, L., Good, C., Fallanca, F., Giovanna Vanoli, E., Ell, P.J., Chan, D., 2015. Simultaneous PET-MRI studies of the concordance of atrophy and hypometabolism in syndromic variants of Alzheimer's disease and frontotemporal dementia: an extended case series. *J. Alzheimers Dis.* 46, 639–653. <http://dx.doi.org/10.3233/JAD-150151>.
- Musiek, E.S., Chen, Y., Korczykowski, M., Saboury, B., Martinez, P.M., Reddin, J.S., Alavi, A., Kimberg, D.Y., Wolk, D.A., Julin, P., Newberg, A.B., Arnold, S.E., Detre, J.A., 2012. Direct comparison of fluorodeoxyglucose positron emission tomography and arterial spin labeling magnetic resonance imaging in Alzheimer's disease. *Alzheimers Dement.* 8, 51–59. <http://dx.doi.org/10.1016/j.jalz.2011.06.003>.
- Mutsaerts, H.J.M.M., van Osch, M.J.P., Zelaya, F.O., Wang, D.J.J., Nordhøy, W., Wang, Y., Wastling, S., Fernandez-Seara, M. a., Petersen, E.T., Pizzini, F.B., Fallatah, S., Hendrikse, J., Geier, O., Günther, M., Golay, X., Nederveen, A.J., Bjørnerud, A., Groote, I.R., 2015. Multi-vendor reliability of arterial spin labeling perfusion MRI using a near-identical sequence: implications for multi-center studies. *NeuroImage* 113, 143–152. doi:<https://doi.org/10.1016/j.neuroimage.2015.03.043>.
- Nasreddine, Z., Phillips, N., Bedirian, V., Charbonneau, S., Whitehead, V., Collin, I., Cummings, J., Chertkow, H., 2005. The Montreal Cognitive Assessment, MoCA: a brief screening tool for mild cognitive impairment. *J. Am. Geriatr. Soc.* 53, 695–699.
- Onyike, C.U., Diehl-Schmid, J., 2013. The epidemiology of frontotemporal dementia. *Int. Rev. Psychiatry* 25, 130–137.
- Rascovsky, K., Hodges, J.R., Knopman, D., Mendez, M.F., Kramer, J.H., Neuhaus, J., Van Swieten, J.C., Seelaar, H., Dopper, E.G.P., Onyike, C.U., Hillis, A.E., Josephs, K.A., Boeve, B.F., Kertesz, A., Seeley, W.W., Rankin, K.P., Johnson, J.K., Gorno-Tempini, M.L., Rosen, H., Prioleau-Latham, C.E., Lee, A., Kipps, C.M., Lillo, P., Piguot, O., Rohrer, J.D., Rossor, M.N., Warren, J.D., Fox, N.C., Galasko, D., Salmon, D.P., Black, S.E., Mesulam, M., Weintraub, S., Dickerson, B.C., Diehl-Schmid, J., Pasquier, F., Deramecourt, V., Lebert, F., Pijnenburg, Y., Chow, T.W., Manes, F., Grafman, J., Cappa, S.F., Freedman, M., Grossman, M., Miller, B.L., 2011. Sensitivity of revised diagnostic criteria for the behavioural variant of frontotemporal dementia. *Brain* 134, 2456–2477. doi:<https://doi.org/10.1093/brain/awr179>.
- Schroeter, M.L., Laird, A.R., Chwiesko, C., Deuschl, C., Schneider, E., Bzdok, D., Eickhoff, S.B., Neumann, J., 2014. Conceptualizing neuropsychiatric diseases with multimodal data-driven meta-analyses — the case of behavioral variant frontotemporal dementia. *Cortex* 57, 22–37. <http://dx.doi.org/10.1016/j.cortex.2014.02.022>.
- Spann, S.M., Kazimierski, K.S., Aigner, S., Kraiger, M., Bredies, K., Stollberger, R., Kraiger, M., Bredies, K., Stollberger, R., Tgv, S., 2017. Spatio-temporal TGV denoising for ASL perfusion imaging. *NeuroImage* 157, 81–96.
- Stekete, R.M.E., Bron, E.E., Meijboom, R., Houston, G.C., Klein, S., Mutsaerts, H.J.M.M., Orellana, C.P.M., de Jong, F.J., van Swieten, J.C., van der Lugt, A., Smits, M., 2015. Early-stage differentiation between presenile Alzheimer's disease and frontotemporal dementia using arterial spin labeling MRI. *Eur. Radiol.* doi:<https://doi.org/10.1007/s00330-015-3789-x>.
- Teipel, S., Drzezga, A., Grothe, M.J., Barthel, H., Chételat, G., Schuff, N., Skudlarski, P., Cavado, E., Frisoni, G.B., Hoffmann, W., Thyrian, J.R., Fox, C., Minoshima, S., Sabri, O., Fellgiebel, A., 2015. Multimodal imaging in Alzheimer's disease: validity and usefulness for early detection. *Lancet Neurol.* 4422. [http://dx.doi.org/10.1016/S1474-4422\(15\)00093-9](http://dx.doi.org/10.1016/S1474-4422(15)00093-9).
- Tosun, D., Schuff, N., Rabinovici, G.D., Ayakta, N., Miller, B.L., Jagust, W., Kramer, J., Weiner, M.M., Rosen, H.J., 2016. Diagnostic utility of ASL-MRI and FDG-PET in the behavioral variant of FTD and AD. *Ann. Clin. Transl. Neurol.* 3, 740–751. <http://dx.doi.org/10.1002/acn3.330>.
- Tzourio-Mazoyer, N., Landeau, B., Papathanassiou, D., Crivello, F., Etard, O., Delcroix, N., Mazoyer, B., Joliot, M., 2002. Automated anatomical labeling of activations in SPM using a macroscopic anatomical parcellation of the MNI MRI single-subject brain. *NeuroImage* 15, 273–289. <http://dx.doi.org/10.1006/nimg.2001.0978>.
- Vercllyte, S., Lopes, R., Lenfant, P., Rollin, A., Semah, F., Leclerc, X., Pasquier, F., Delmaire, C., 2015. Cerebral hypoperfusion and hypometabolism detected by arterial spin labeling MRI and FDG-PET in early-onset Alzheimer's disease. *J. Neuroimaging.* <http://dx.doi.org/10.1111/jon.12264>.
- Verfaillie, S.C.J., Adriaanse, S.M., Binnewijzend, M.A.A., Benedictus, M.R., Ossenkoppele, R., Wattjes, M.P., Pijnenburg, Y.A.L., van der Flier, W.M., Lammertsma, A.A., Kuijter, J.P.A., Boellaard, R., Scheltens, P., van Berckel, B.N.M., Barkhof, F., 2015. Cerebral Perfusion and Glucose Metabolism in Alzheimer's Disease and Frontotemporal Dementia: Two Sides of the Same.
- Vidorreta, M., Wang, Z., Rodríguez, I., Pastor, M.A., Detre, J.A., Fernández-Seara, M.A., 2013. Comparison of 2D and 3D single-shot ASL perfusion fMRI sequences. *NeuroImage* 66, 662–671. <http://dx.doi.org/10.1016/j.neuroimage.2012.10.087>.
- Weder, N.D., Aziz, R., Wilkins, K., Tampi, R.R., 2007. Frontotemporal dementias: a review. *Ann. General Psychiatry* 6, 15. <http://dx.doi.org/10.1186/1744-859X-6-15>.
- Weyts, K., Vernooij, M., Stekete, R., Valkema, R., Smits, M., 2017. Qualitative agreement and diagnostic performance of arterial spin labelling MRI and FDG PET-CT in suspected early-stage dementia. *Clin. Imaging* 45, 1–7. <http://dx.doi.org/10.1016/j.clinimag.2017.05.008>.
- Yeo, J.M., Lim, X., Khan, Z., Pal, S., 2013. Systematic review of the diagnostic utility of SPECT imaging in dementia. *Eur. Arch. Psychiatry Clin. Neurosci.* 263, 539–552. <http://dx.doi.org/10.1007/s00406-013-0426-z>.
- Zaharchuk, G., Bammer, R., Straka, M., Shankaranarayan, A., Alsop, D.C., Fischbein, N.J., Atlas, S.W., Moseley, M.E., 2009. Arterial spin-label imaging in patients with normal bolus perfusion-weighted MR imaging findings: pilot identification of the borderzone sign. *Radiology* 252, 797–807. <http://dx.doi.org/10.1148/radiol.2523082018>.
- Zhang, Y., Schuff, N., Ching, C., Tosun, D., Zhan, W., Nezamzadeh, M., Rosen, H.J., Kramer, J.H., Gorno-Tempini, M.L., Miller, B.L., Weiner, M.W., 2011. Joint assessment of structural, perfusion, and diffusion MRI in Alzheimer's disease and frontotemporal dementia. *Int. J. Alzheimers Dis.* 2011, 546871. <http://dx.doi.org/10.4061/2011/546871>.